

# Direct Reconstruction of the Dark Energy Scalar-Field Potential

Chao Li<sup>1</sup>, Daniel E. Holz<sup>2,3</sup>, Asantha Cooray<sup>4</sup>

<sup>1</sup>*California Institute of Technology, Mail Code 130-33, Pasadena, CA 91125*

<sup>2</sup>*Theoretical Division, Los Alamos National Laboratory, Los Alamos, NM 87545, and Department of Astronomy & Astrophysics, University of Chicago, Chicago, IL 60637*

<sup>3</sup>*The Observatories of the Carnegie Institution of Washington, Pasadena, CA 91101*

<sup>4</sup>*Center for Cosmology, Department of Physics and Astronomy, University of California, Irvine, CA 92697*

(Dated: December 24, 2018)

While the accelerated expansion of the Universe is by now well established, an underlying scalar field potential possibly responsible for this acceleration remains unconstrained. We present an attempt to reconstruct this potential using recent SN data, under the assumption that the acceleration is driven by a single scalar field. Current approaches to such reconstructions are based upon simple parametric descriptions of either the luminosity distance or the dark energy equation of state. We find that these various approximations lead to a range of derived evolutionary histories of the dark energy equation of state (although there is considerable overlap between the different potential shapes allowed by the data). Instead of these indirect reconstruction schemes, we discuss a technique to determine the potential directly from the data by expressing it in terms of a binned scalar field. We apply this technique to a recent SN dataset, and compare the results with model-dependent approaches. In a similar fashion to direct estimates of the dark energy equation of state, we advocate direct reconstruction of the scalar field potential as a way to minimize prior assumptions on the shape, and thus minimize the introduction of bias in the derived potential.

## I. INTRODUCTION

Distance estimates to Type Ia supernovae (SNe) are currently a preferred probe of the expansion history of the Universe [1], and have led to the discovery that the expansion is accelerating [2]. It is now believed that a mysterious dark energy component, with an energy density  $\sim 70\%$  of the total energy density of the universe, is responsible for the accelerated expansion [3]. While the presence of acceleration is now well established by various cosmological probes, the underlying physics remains a complete mystery. As the precise nature of the dark energy has profound implications, understanding its properties is one of the biggest challenges today.

With the advent of large surveys for Type Ia supernovae, such as the Supernova Legacy Survey (SNLS) [26] and Essence [27], among others, it is hoped that we will study details of the expansion, and thereby elucidate the physics responsible for the acceleration. Under the assumption that the dark energy is due to a single scalar field rolling down a potential, several studies have considered how future data might be used to reconstruct the potential, either based on various analytical descriptions of the luminosity distance [4], or through specific assumptions about the potential, such as a polynomial function in the scalar field [5]. It is already well established that certain parametric descriptions of the distance lead to biased estimates for the dark energy equation-of-state (EOS) and the potential [7]. While improved parametric forms of fitting functions have been suggested [8, 10], it is unclear how to select an optimal approach for reconstructing the dark energy scalar field potential from SN distances (for a review of various possibilities, see Ref. [11]).

In this paper we discuss issues related to potential and

dark energy EOS reconstruction by making use of a recent set of SN data from the SNLS survey [12]. The sample includes 73 high redshift SNe complemented with a sample of 44 nearby supernovae [12]. We compare and contrast a variety of methods to reconstruct the potential and the dark energy EOS. We write the luminosity distance either as a simple polynomial expansion in redshift, or as a Padé approximant [13] (which avoids some of the known problems in the polynomial expansion when taking derivatives [7, 8, 14]). In addition to approximating the luminosity distance, we also explore two approximations to the EOS:  $w(z) = w_0 + w_a(1 - a)$  [16] and  $w(z) = w_0 - \alpha \ln(1 + z)$  [8].

Based on our model reconstruction of the potential, we find that while there is significant overlap of the allowed  $V(\phi)$  region favored by each of the four reconstruction methods, the models give rise to different histories for the EOS, especially within the two parameter plane,  $w-w'$  (the EOS parameter,  $w$ , and its time derivative,  $w' \equiv dw/d\ln a$ , as functions of redshift [17]). We argue that existing parametric fitting functions for either distance or the EOS lead to biased reconstructions of the potential. In the literature, however, there exist model-independent approaches to the reconstruction of the dark energy density [18] and the EOS [19], which bin the parameters directly as a function of redshift, with the number and width of the bins determined by the statistical quality of data. These estimates can also be arranged to be uncorrelated [19], allowing unique insights into the evolution without being subject to prior assumed redshift dependencies. Here we suggest a similar model-independent approach to the reconstruction of the scalar potential from SN data. Instead of utilizing a polynomial expansion for the potential [5], which assumes a limited range of models (once the expansion is truncated at a

certain order), we propose a binning scheme for the potential that can be applied to data with a minimal, and easily controlled and understood, number of assumptions for the potential shape.

The paper is organized as follows: In the next Section we review techniques for reconstructing the scalar-field potential from SN distances. We also reconstruct the EOS as a function of redshift, and use this to study the  $w-w'$  plane (which has been advocated as a way to characterize the underlying potential responsible for the dark energy component by separating the regime into “freezing” and “thawing” potentials [17]; see, also [20] for a Monte-Carlo exploration). In Section III we explore the impact of different parameterizations on the derived evolutionary histories. While we observe these differences with  $\sim 115$  SN data points, future large SN datasets may lead to apparently inconsistent results. In Section IV, following the approach to model-free estimates of the dark energy EOS [19], we present a model-independent estimate of the scalar field potential. We conclude with a summary of our main results in Section V.

## II. POTENTIAL VIA PARAMETRIC FORMS

For this study we make use of SN data from SNLS [12]. Due to complications related to independent data sets (e.g., differing calibration, color correction, extinction correction, etc.), we do not attempt to increase the sample size by combining other SN datasets. The measurements from Ref. [12] present the quantity  $\mu_B = m_B - M$  for 117 SNe, with 73 of these at redshifts greater than 0.2 [28]. This distance modulus is related to the luminosity distance through  $\mu_B = 5 \log_{10} d_L$ , while the luminosity distance is related to the comoving radial distance via  $d_L = c(1+z)r(z)/H_0$ , where  $r(z) = \int_0^z dz'/H(z')$  with  $H(z)$  the expansion rate of the Universe. When model fitting the data, we fix  $\mathcal{M} = 19.3 \pm 0.03$  to the value determined by SNLS. We take the central value; further uncertainty will be incorporated into  $\sigma_{\text{int}}$ , as discussed below.

In our reconstruction of the potential, we describe  $r(z)$  through two parametric forms widely used in the literature. First, we expand  $r(z)$  as a simple power-law [4] such that

$$r(z) = z + a_2 z^2 + a_3 z^3 + a_4 z^4. \quad (1)$$

Note that the coefficient of the first order term is exactly one. Since this polynomial expansion has known problems when estimating the derivatives of  $r(z)$  (e.g., Figure 3 of [8], and also [9]), we also consider a Padé form for  $r(z)$  with [13]:

$$r(z) = 2 \frac{z + c_1(1 - \sqrt{1+z})}{c_2(1+z) + c_3\sqrt{1+z} + 2 - c_1 - c_2 - c_3}, \quad (2)$$

such that as  $z \rightarrow 0$ ,  $r(z) \rightarrow z$ . In this form, using  $r(z \rightarrow$

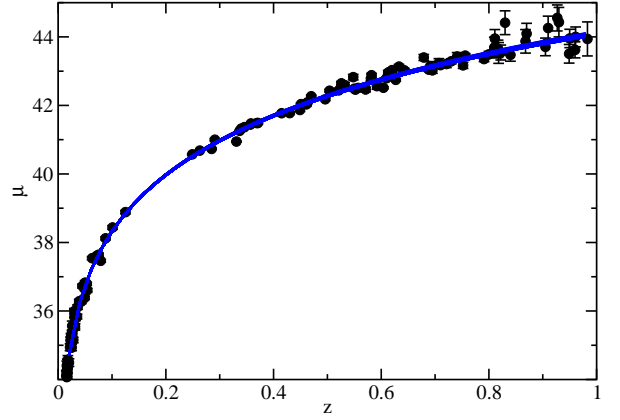


FIG. 1: Hubble diagram for 115 Type Ia SNe used in the present analysis. The error bars are on  $\mu_B$  only. We also include an additional constant error,  $\sigma_{\text{int}} = 0.13$ , to account for the SN intrinsic dispersion. For reference we also plot 300 curves drawn uniformly from the  $2\sigma$  consistent likelihood fits to the data using the Taylor expansion with  $r(z) = z + a_2 z^2 + a_3 z^3 + a_4 z^4$ .

$\infty$ ), one can additionally constrain the parameters with:

$$\begin{aligned} 3\Omega_M &\leq \frac{4c_2 + 2c_3 - c_1}{2 - c_1} \\ 1 \leq \frac{1}{c_2} &\leq \frac{1}{2} \int_1^\infty \frac{dx}{\sqrt{1 - \Omega_M + \Omega_M x^3}}. \end{aligned} \quad (3)$$

In addition to the two fitting forms for  $r(z)$ , we also determine  $r(z)$  through model parameterizations for  $w(z)$ , including  $w(z) = w_0 + (1-a)w(a)$  [15, 16] and  $w(z) = w_0 + \alpha \ln(1+z)$  [8]. Since from  $w$  it is possible to determine the distance, these approximations allow us to once again reconstruct the dark energy potential.

In each of two parametric descriptions of  $r(z)$  we have three free parameters. We parameterize  $w(z)$  with two parameters, and include  $\Omega_m$  as a third free parameter (under the assumption of a flat universe; weakening this assumption significantly degrades our ability to measure anything about the potential with existing data). When showing results related to potentials or EOS as a function of redshift, we take a prior on  $\Omega_m$  such that the probability is Gaussian with a mean of 0.25 and a standard deviation given by  $\sigma = 0.05$  [3]. In each case, to obtain the joint likelihood distribution of the parameters given the data, we perform a likelihood analysis:

$$\chi^2(p_i) = \sum_{i=1}^N \frac{[\mu - \mu_B(z_i)]^2}{\sigma_{\mu_B}^2 + \sigma_{\text{int}}^2}, \quad (4)$$

where, following Ref. [12], in addition to statistical uncertainty in  $\mu_B$  we include an additional Gaussian uncertainty,  $\mu_{\text{int}} = 0.13$ , representing the intrinsic dispersion

of SN absolute magnitudes,  $M$ . We ignore complications related to covariances in the Hubble diagram, either due to effects related to calibration [23] or fundamental limitations such as gravitational lensing correlation of SN flux [24] or peculiar velocities [25]. The posterior probability distribution is taken to be  $P(p_i|\mu) \propto e^{-\frac{1}{2}\chi^2(p_i)}$ , and we marginalize the likelihood over the uncertainty in  $\Omega_m$ , assuming a Gaussian prior Gaussian.

Once the joint probability distribution for parameters is determined, we sample the  $1\sigma$  and  $2\sigma$  range allowed by these parameters to draw a fixed ( $> 600$ ) number of independent  $r(z)$  curves consistent with the data. For each of these distance curves,  $r_i(z)$ , we obtain the scalar-field potential, in dimensionless units such that  $\tilde{V}(\tilde{\phi}) = V(\phi)/\rho_{\text{crit}} = V/(3H_0^2/8\pi G)$ , through [4]

$$\tilde{V}(\tilde{\phi}) = \left[ \frac{1}{(d\tilde{r}/dz)^2} + \frac{1+z}{3} \frac{d^2\tilde{r}/dz^2}{(d\tilde{r}/dz)^3} \right] - \frac{1}{2} \Omega_M (1+z)^3, \quad (5)$$

where  $\tilde{r} = H_0 r$ . For each of the  $r_i(z)$  estimates, we also randomly draw  $\Omega_m$  from a Gaussian prior distribution as described above. The mapping between  $z$  and  $\phi$ , the scalar field value, is obtained through

$$\begin{aligned} \frac{d\tilde{\phi}}{dz} &= -\frac{d\tilde{r}/dz}{(1+z)} \\ &\times \left[ -\frac{1}{4\pi} \frac{(1+z)d^2\tilde{r}/dz^2}{(d\tilde{r}/dz)^3} - \frac{3}{8\pi} \Omega_M (1+z)^3 \right]^{1/2} \end{aligned} \quad (6)$$

where  $\tilde{\phi} = \phi/m_{\text{Pl}}$ . Furthermore, for models where we parameterize  $r(z)$ , we can also extract the dark energy EOS as

$$w(z) = \frac{1+z}{3} \frac{3\Omega_m(1+z)^2 + 2(d^2r_i/dz^2)/(dr_i/dz)^3}{\Omega_m(1+z)^3 - (dr_i/dz)^{-2}} - 1. \quad (7)$$

When selecting models associated with scalar fields, we require that  $\partial\phi/\partial z > 0$ , such that  $w \geq -1$ . Even in the case of  $w(z)$  parameterizations where model fits allow  $w < -1$ , we ignore  $w(z)$  below this value as single scalar-field models do not naturally give rise to such equations-of-state.

### III. BIASES IN MODEL-DEPENDENT ESTIMATES

In Fig. 1 we show the Hubble diagram for the 115 data points from Ref. [12] used in this analysis. For reference, we also plot  $\sim 300$  distance curves which are  $2\sigma$  consistent curves drawn from the likelihood distribution for parameters under the Taylor expansion for  $r(z)$ . The best-fit model with this parameterization has a chi-square value of 113.1 with 112 degrees of freedom. Note that in Ref. [12],  $\sigma_{\text{int}}$  is tuned so that  $\chi^2 = 1$  for the best-fit model under standard- $\Lambda$ CDM cosmological fits to the

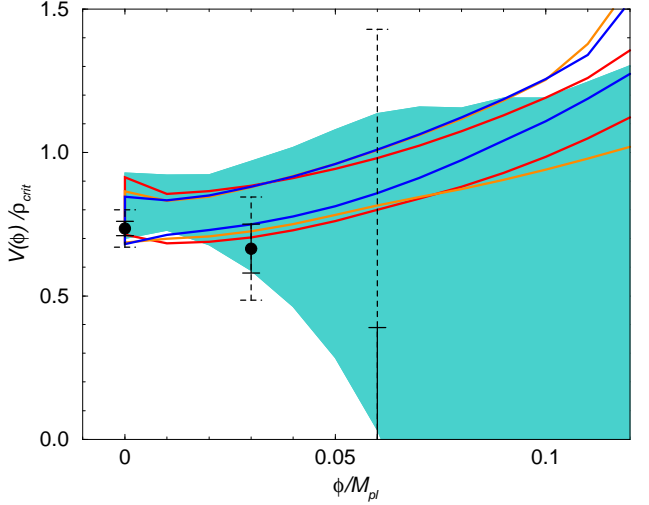


FIG. 2: The normalized quintessence potential  $\tilde{V}(\phi)$  vs  $\phi/m_{\text{Pl}}$ . The shaded region is allowed at the  $2\sigma$  confidence level when using the Taylor expansion for  $r(z)$ . The red lines mark the same when using a Padé approximation to the distance. The orange and blue lines are for the cases where  $w(z)$  is parameterized by  $w(z) = w_0 + \alpha \ln(1+z)$  and  $w(z) = w_0 + w_a(1-a)$ , respectively. Here  $\phi = 0$  corresponds to  $z = 0$ , while  $\phi > 0.1$  generally corresponds to  $z > 1$  (depending on  $d\phi/dz$ ). The points with error bars show the  $1\sigma$  (solid) and  $2\sigma$  (dashed) model-independent estimates of the potential described in Section IV (see equation (8)). While there is considerable overlap in the allowed region, there are also significant differences in terms of the redshift evolution of the EOS.

data. We use their best-fit value,  $\sigma_{\text{int}} = 0.13$ , and do not take this intrinsic uncertainty as an additional free parameter in our modeling. The exact value of the intrinsic dispersion does not impact our comparison of different approaches to the reconstruction of the quintessence potential. It is to be emphasized that all of our parameterizations of either distance or the EOS yield comparable  $\chi^2$  values for the best-fit model. This suggests that all four of the reconstruction methods outlined above are indistinguishable within the redshift range considered.

As discussed in the previous section, for each of the four parameterizations we determine a best-fit  $r(z)$  to the SN data. We then Monte-Carlo generate models within  $2\sigma$  of this best-fit, generating over 600 instances of  $w(z)$  and  $V(\phi)$ , all of which are consistent with the underlying SN dataset at the  $2\sigma$  level. In Fig. 2 we show the potentials reconstructed from each of the four methods, with the bands encapsulating 95% of the distribution of the individual models. Due to the behavior of the Taylor expansion at high  $z$ , and the fact that we do not restrict the coefficients of the polynomial expansion to follow a flat universe, this parameterization gives rise to a large range of acceptable potentials which satisfy the data. The Padé parameterization of  $r(z)$ , as well as the  $w(z)$  models, significantly improve the constraints on allowed potential shapes. This is because the parameters in

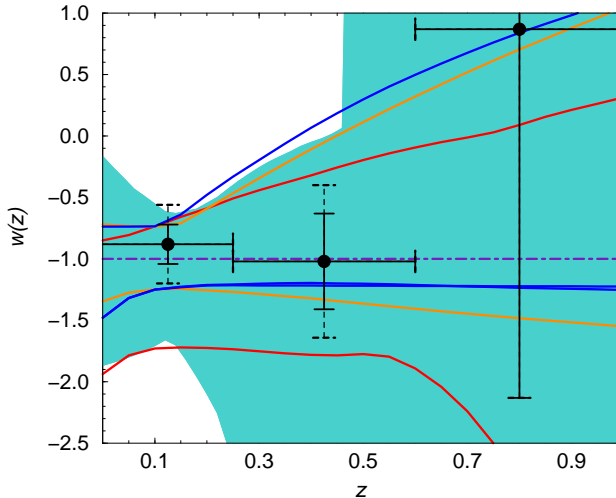


FIG. 3: The dark energy EOS,  $w(z)$ , as a function of redshift. The curves show the  $2\sigma$  allowed values and correspond to the potentials shown in Fig. 2. Note that if we impose  $\partial\phi/dz > 0$ , then  $w > -1$ , as single scalar-field models do not lead to  $w < -1$ . However, as shown, most of the parameterizations allow the region below  $w < -1$ . When constructing the potentials shown in Fig. 2, we apply the condition that  $\partial\phi/dz > 0$ . Note that the  $w(z)$  parameterizations, with two free parameters, are the most restrictive parameterization in the regime  $z < 0.3$ . Over the redshift range probed, the different parameterizations generally agree with each other. The plotted error bars show the  $1\sigma$  and  $2\sigma$  errors of  $w_i(z)$  when the EOS is subdivided into three bins in redshift, with  $w_i(z)$  directly measured from data and no restrictions on its values. A Gaussian prior has been taken on  $\Omega_m$  with a one sigma uncertainty of 0.05 with  $w(z)$  parameterizations.

the Padé approximation are additionally constrained to satisfy criteria related to the behavior of  $r(z)$  as  $z \rightarrow \infty$ , as well as by the assumption of a flat universe. When fitting the  $w(z)$  parameterizations to the data, we were able to impose a prior on  $\Omega_m$  based on existing cosmological information (this was not possible when using  $r(z)$  fitting functions). While we find some overlap in the  $2\sigma$  allowed region in the  $\phi$ - $V(\phi)$  plane between the four approaches, there are also noticeable inconsistencies. Analyses of an identical dataset with different approximations to  $V$  or  $w$  lead to differing resulting best-fit potentials.

The differences related to potential shapes between the four methods are best captured in terms of evolutionary histories for the dark-energy EOS. In Fig. 3 we summarize the best-fit  $w(z)$  results for each of the four reconstruction techniques. Note that some of our parameterizations allow  $w(z) < -1$ , but due to our assumption that the dark energy arises from a scalar-field potential where  $w(z)$  is always expected to be greater than -1, we restrict the allowed parameter space to be the region where  $w(z) > -1$ . Similarly to Fig. 2, we find considerable overlap between different reconstruction schemes in the  $w(z)$  versus redshift plane, with most models indicating that as the redshift is decreased,  $w(z)$  tends to values

between -0.8 and -1.0 at  $z = 0$ . In terms of our direct  $w(z)$  parameterizations, with  $w(z) = w_0 + (1-a)w_a$  we find  $w_0 = -1.12 \pm 0.14$  and  $w_a = 0.38 \pm 0.49$  at the  $68\%$  confidence level. In the case of  $w(z) = w_0 + \alpha \ln(1+z)$  we find  $w_0 = -1.08 \pm 0.11$  and  $\alpha = -0.4 \pm 0.75$ . As shown in prior studies [14],  $w(z)$  parameterizations allow for a minimum  $w(z)$  region at a certain pivot redshift. For the dataset used here, this pivot redshift is at  $z \sim 0.12$ , and at the  $2\sigma$  confidence level we find that the pivot point satisfies  $-1.23 < w_p \equiv w(z=0.12) < -0.74$ , using  $w(z) = w_0 + (1-a)w_a$ . It is important to note that all the parameterizations are consistent with a cosmological constant.

In Figs. 2 and 3 we show the  $2\sigma$  bands of best-fit models to the data, under different parametrizations of the distance or dark energy EOS. In addition to this outer envelope, we are also interested in the distribution of the individual  $w(z)$  models within the  $2\sigma$  bands. We thus study the behavior of the models in the  $w$ - $w'$  plane, which has been suggested as a natural venue in which to distinguish models [17]. We Monte-Carlo 600 scalar potentials,  $V(\phi)$ , and evolution histories,  $w(z)$ , within the  $2\sigma$  regime of the best-fit parameters for each of the four fitting functions. In Fig. 4 we plot  $w$  and  $w'$  at  $z = 0.1$  and  $z = 0.5$  for each Monte-Carlo model, with the scatter of points being  $2\sigma$  consistent with our underlying SN data set.

Based on the evolutionary behavior of simple scalar-field models in the  $w$ - $w'$  plane, it has been suggested that one can separate potentials into “thawing” and “freezing” regions, based upon their shapes [17]. These regions are delineated in Fig. 4, for comparison with our individual Monte-Carlo models. It is apparent that the different parametrization approaches yield separate, though often overlapping, regions within the  $w$ - $w'$  plane. In addition, the models are not necessarily well-contained within the thawing or freezing regions, with a freezing model in one parametrization ending up as a thawing model in another, or with models ending up in between thawing or freezing, or well outside of either regime. Using generic numerical models for the potential shape, this behavior has also recently been highlighted in [20]. By applying additional constraints on allowable potentials (especially at high  $z$ ), [17] find much tighter confinement in the  $w$ - $w'$  plane.

Any statement regarding the shape of the scalar potential, as determined from data, is thus crucially dependent upon the underlying parametrizations. For example, for the Taylor expansion approach  $w'$  is largely negative at  $z = 0.5$ , while it is positive at  $z = 0.1$ . Under the Padé approximation,  $w'$  is negative at both  $z = 0.1$  and  $z = 0.5$ , with  $w$  tightly clustered ( $-0.9 \lesssim w \lesssim -0.8$ ) at  $z = 0.1$  and relatively unconstrained at  $z = 0.5$ . Although the reconstructed potentials show significant overlap (see Fig. 2), the distributions in the  $w$ - $w'$  plane are less consistent among different parameterizations. Thus, while there is motivation from theoretical arguments for using the  $w$ - $w'$  plane for potential recognition,

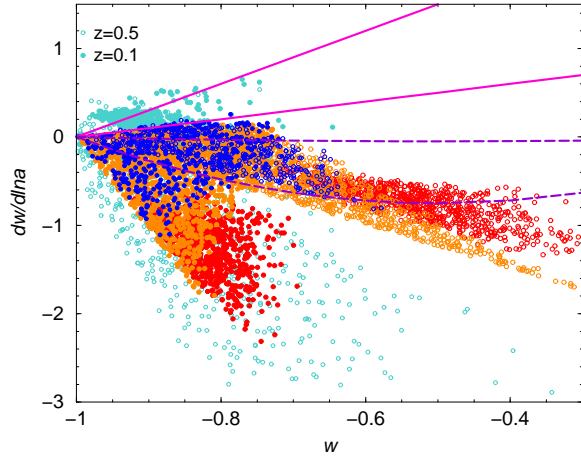


FIG. 4:  $w$  versus  $dw/d \ln a$ . The data points show the EOS and its time derivative for 600 model potentials uniformly drawn at the  $2\sigma$  confidence level at redshift of 0.1 (filled symbols) and 0.5 (open symbols). The cyan, red, orange, and blue data points show potentials selected under the Taylor expansion, Padé approximation,  $w(z) = w_0 + \alpha \ln(1+z)$  and  $w(z) = w_0 + w_a(1-a)$  model fits to the data, respectively. For comparison, we also plot the thawing (dashed) and freezing (solid) potential regions, following Ref. [17]. There are considerable differences in  $w$  and  $dw/d \ln a$  values, and the evolution captured by two redshifts, between the four approaches. These values do not satisfy the expectations under simple model criteria for the dark energy potentials, though all of these potentials, and the  $w(z)$  curves, are consistent with the data at the  $2\sigma$  confidence level.

there is no obvious, parametrization independent way to convert distance data to constraints in this plane.

The differences seen in Fig. 4 are attributable to the different parametric forms used to approximate the distance or the dark energy EOS. To paraphrase our results: you get out what you put in. Furthermore, the fitting forms to both the distance and the EOS are motivated by their ability to fit data, and possess no clear physical motivation. Fig. 4 thus emphasizes the need for an approach which makes minimal assumptions about the underlying potential, thereby maximizing the measurement of a completely unknown scalar field. The less we assume about the potential, the more powerful the ensuing measurement of its shape. Such an approach is presented in the following section.

#### IV. MODEL-FREE ESTIMATES

Thus far we have discussed results based on assumed parameterizations for either distance or dark energy EOS. These parameterizations lead to conclusions that are subject to the assumed parameterizations. It is desirable to make model independent estimates of dark energy. In the case of the EOS  $w(z)$ , one could approach this by binning  $w(z)$  in redshift [19]. Applying this to our SNLS dataset, we evaluate  $w(z)$  over three bins in red-

shift,  $0 < z_1 < 0.25$ ,  $0.25 < z_2 < 0.6$ , and  $0.6 < z_3 < 1.0$ , assuming  $w(z_i)$  constant in each bin.

The resulting best-fit to the SN data is shown by the data points with  $1\sigma$  and  $2\sigma$  error bars in Fig. 3. We find  $w(z_1) = -0.88 \pm 0.28$  and  $w(z_2) = -1.02^{+0.94}_{-1.26}$  with no useful constraint for  $w(z)$  in the  $z_3$  bin. Although these bins are correlated at the 10% level, it is possible to decorrelate the binned  $w_i(z)$  estimates following the approach of Ref. [19]. While only three bins are attempted here, as SN sample sizes increase, one can consider larger numbers of bins, each narrower in redshift. The estimates shown in Fig. 3 are consistent with estimates based on both fitting functions to the EOS,  $w(z) = w_0 + w_a(1-a)$  and  $w(z) = w_0 + \alpha \ln(1+z)$ . As discussed in Ref. [19], the binned estimates capture the dark energy EOS with minimal prior assumptions on the parameterization. This is expected to maximize the information one can extract from the data, while minimizing the introduction of biases.

As discussed and noted elsewhere [7, 8], the scalar-field potential reconstruction is also subject to prior assumptions on the fitting form. To avoid biases and to make statements that are not subject to assumed parameterization, it is useful to directly construct the potential from data. Recent approaches in the literature consider fitting distance data to a potential expanded as a polynomial in the scalar field with  $V(\phi) = \sum_{i=0}^{\infty} V_i \phi^i$  [5, 6, 20]. Since we are forced to truncate the expansion at low order (for example, at cubic order with existing data [5]), the potential is no longer arbitrary, but rather has a very limited range of possible shapes.

Instead of assuming a specific family of shapes for  $V(\phi)$ , we propose a “model-free” extraction of the potential directly from the data. We make two assumptions about the scalar field potential: (1) that it is a piecewise continuous function, and (2) that its structure is “uniform” in the  $\phi$  range explored by the data. For  $(N-1)\Delta\phi < \phi < N\Delta\phi$ , we describe the potential as a function of the field with constant gradients,  $dV/d\phi$ , over binned intervals,  $\Delta\phi$ :

$$V(\phi) = V_0 + \sum_{i=1}^{N-1} (dV/d\phi)_i \Delta\phi + (\phi - (N-1)\Delta\phi)(dV/d\phi)_N. \quad (8)$$

Assumption (1) above ensures continuity of  $V(\phi)$ , which is necessary since one evolves the potential through the dynamic equation for the field as  $\ddot{\phi} + 3H\dot{\phi} + dV/d\phi = 0$ , and discontinuities would lead to infinite derivatives. This requirement is unnecessary when considering parameter-free estimates of the dark energy EOS, which is allowed discontinuous jumps in redshift. Both the constant-value and the constant-slope approaches to parametrizing the dark energy EOS lead to similar conclusions [19]. Assumption (2) states that our bins in  $\phi$  are fixed width:  $\Delta\phi$  is a constant, independent of  $\phi$ . This assumption could be relaxed (e.g., finer bins near  $\phi = 0$ ), but this would lead to additional parameters, in addition to introducing model-dependent assumptions

into the analysis. The expansion of  $V(\phi)$  in Eq. 8 appears to make the least offensive assumptions possible, and thereby offers the basis with which to maximally constrain the full range of possible underlying potentials.

We apply the above potential description to SNLS data following the same approach as Ref. [5], with three free parameters:  $V_0$ ,  $(dV/d\phi)_1$  for  $0 < \phi < 0.03$ , and  $(dV/d\phi)_2$  for  $\phi > 0.03$ . The sizes of the bins are chosen by the range of  $\phi$  we are able to constrain, which is in turn related to both the redshift range of the SN dataset and the shape of the potential. Note that we take  $\phi = 0$  to coincide with  $z = 0$ . Instead of  $(dV/d\phi)_2$ , we convert the gradient to a data point at  $\phi = 0.06$ , although we find only an upper limit, as this gradient is not strongly constrained by existing data. In Fig. 2 we show the estimated potential and error bars at the  $1\sigma$  and  $2\sigma$  level. The potential values allowed by the data are generally consistent with other indirect reconstructions based on fitting forms for the distance or the EOS. While fitting forms lead to largely positive  $V(\phi)$  at  $\phi > 0.05$ , our binned approach finds only an upper limit in this range.

While we have described the potential with only three parameters, this can be straightforwardly generalized to additional bins as the statistics and quality of the SN samples improve. In addition, we make a minimal number of assumptions regarding the potential, and thus are not biased for or against any particular shapes for the scalar field potential. The proposed approach is similar to the case where the EOS is binned and directly measured from the data without specifying a model for the evolution. As SN data samples increase in size, we believe such a model independent approach will become a powerful tool in extracting information about underlying scalar field potentials.

## V. SUMMARY

We have presented a reconstruction of a single scalar-field potential using recent SN data from the SNLS survey [12]. We have shown that reconstructions based on various approximations to the distance and the EOS lead to differing evolution histories of the dark energy EOS, particularly when the models are examined in the  $w-w'$  plane. In this plane the same data can lead to large

movements in best-fit models, depending on the specific approximations to distance or EOS which are being utilized. Thus the underlying model assumptions lead to biases, compromising our ability to distinguish evolutionary behaviors of the dark energy. At present the models are only weakly constrained by the data, and thus this model-dependence, although apparent, is not a critical failure. As the data improves, however, a model-independent approach will be essential to determining an otherwise completely unknown scalar-field potential.

As an alternative to existing indirect reconstruction schemes, we have thus proposed a technique which establishes the potential directly from the data, with only minimal assumptions about the underlying shape of the potential. We take the potential to be a binned scalar field, piecewise linear and continuous, but otherwise completely arbitrary. Given the simplicity of these assumptions, this potential is unlikely to introduce biases in the determination of a completely unconstrained, underlying potential. We have demonstrated this approach with current SN data, comparing the results to parametrized analyses. The ensuing constraints, although weaker, are expected to be robust and unbiased. It has been found that direct binning approaches to the dark energy EOS hold great promise for establishing model-independent measurements [19]. We propose a similar approach to reconstructing the underlying dark energy scalar field potential, allowing us to make assumption-free statements about the nature of the completely unknown and mysterious field potentially responsible for the accelerating expansion of the Universe.

## VI. ACKNOWLEDGMENTS

AC and DEH are partially supported by the DOE at LANL through IGPP grant Astro-1603-07. DEH acknowledges a Richard P. Feynman Fellowship from LANL, and is grateful to the Moore Center for Theoretical Cosmology and Physics at Caltech for its hospitality. CL is supported by the Gordon Moore Foundation at Caltech. We thank Dragan Huterer for useful discussions related to this work, and Eric Linder and Robert Caldwell for very detailed comments on an earlier version of the paper.

---

[1] A. G. Riess *et al.*, B. J. Barris *et al.*, arXiv:astro-ph/0310843; R. A. Knop *et al.*, arXiv:astro-ph/0309368; J. L. Tonry *et al.*, *Astrophys. J.* **594**, 1 (2003).

[2] S. Perlmutter *et al.*, *Astrophys. J.* **517**, 565 (1999); A. Riess *et al.*, *Astron. J.* **116**, 1009 (1998).

[3] D. N. Spergel *et al.* [WMAP Collaboration], *Astrophys. J. Suppl.* **148**, 175 (2003);

[4] D. Huterer and M. S. Turner, *Phys. Rev. D* **60** 081301 (1999).

[5] M. Sahlen, A. R. Liddle and D. Parkinson, *Phys. Rev. D* **72**, 083511 (2005) [arXiv:astro-ph/0506696].

[6] M. Sahlen, A. R. Liddle and D. Parkinson, [arXiv:astro-ph/0610812].

[7] J. Weller and A. Albrecht, *Phys. Rev. D* **65**, 103512 (2002) [arXiv:astro-ph/0106079].

[8] B. F. Gerke and G. Efstathiou, “Probing quintessence: Reconstruction and parameter estimation from Mon. Not. Roy. Astron. Soc.” **335**, 33 (2002) [arXiv:astro-ph/0201336].

[9] J. Jonsson, A. Goobar, R. Amanullah, and L. Bergstrom,

JCAP **09**, 007 (2004)

[10] Z. K. Guo, N. Ohta and Y. Z. Zhang, Phys. Rev. D **72**, 023504 (2005) [arXiv:astro-ph/0505253].

[11] V. Sahni and A. Starobinsky, arXiv:astro-ph/0610026.

[12] P. Astier et al., Astron. Astrophys. **447** 31 (2006), astro-ph/0510447.

[13] T. D. Saini, S. Raychaudhury, V. Sahni and A. A. Starobinsky, Phys. Rev. Lett. **85**, 1162 (2000) [arXiv:astro-ph/9910231].

[14] D. Huterer and M. S. Turner, Phys. Rev. D **71**, 123527 (2001).

[15] M. Chevallier, D. Polarski Int. J. Mod. Phys. D **10**, 213 (2001) [arXiv:gr-qc/0009008]

[16] E. V. Linder, Phys. Rev. Lett. **90** 091301 (2003)

[17] R. R. Caldwell and E. V. Linder, Phys. Rev. Lett. **95**, 141301 (2005) [arXiv:astro-ph/0505494].

[18] Y. Wang and M. Tegmark, Phys. Rev. D **71**, 103513 (2005) [arXiv:astro-ph/0501351].

[19] D. Huterer and A. Cooray, Phys. Rev. D **71**, 023506 (2005) [arXiv:astro-ph/0404062].

[20] D. Huterer and H. V. Peiris, arXiv:astro-ph/0610427.

[21] S. Nojiri, S. Odintsov and H. Stefancic, Phys. Rev. D **74**, 086009 (2006); S. Nojiri, S. Odintsov and M. Sami Phys. Rev. D **74**, 046004 (2006)

[22] C. Schimd et.al., [arXiv:astro-ph/0603158].

[23] A. G. Kim and R. Miquel, Astropart. Phys. **24**, 451 (2006) [arXiv:astro-ph/0508252].

[24] A. Cooray, D. Huterer and D. Holz, Phys. Rev. Lett. **96**, 021301 (2006) [arXiv:astro-ph/0509581].

[25] L. Hui and P. B. Greene, Phys. Rev. D **73**, 123526 (2006) [arXiv:astro-ph/0512159]; A. Cooray and R. R. Caldwell, Phys. Rev. D **73**, 103002 (2006) [arXiv:astro-ph/0601377].

[26] <http://www.cfht.hawaii.edu/SNLS/>

[27] <http://www.ctio.noao.edu/~wsne/>

[28] The distance estimates for two high-redshift SNe lie more than  $3\sigma$  away from the best-fit relation in the Hubble diagram. As in Ref. [12], we exclude these two data points and only make use of 115 data points to model fit the data.